Engineering Structures 231 (2021) 111844

Contents lists available at ScienceDirect

Engineering Structures

journal homepage: www.elsevier.com/locate/engstruct

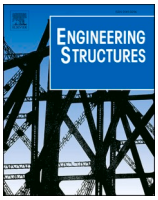

Structural response analysis of explosions in hydrogen-air mixtures in tunnel-like geometries

Magne Bratland *, Dag Bjerketvedt, Knut Vaagsaether

Department of Process, Energy and Environmental Technology, University of South-Eastern Norway, Kjoelnes ring 56, N-3918 Porsgrunn, Norway

ARTICLE INFO

Keywords:
Explosions
Hydrogen
Tunnels
Channels
Shock response spectrum

ABSTRACT

This paper presents a structural response analysis based on the results of experiments involving gas explosions in inhomogeneous hydrogen-air mixtures in a channel. The channel was 3 m long, with a cross-section of 100 mm by 100 mm, and open at one end. Hydrogen was released into the channel using 0.25 mm and 0.5 mm ID nozzles.

Strong and relatively prolonged pressure oscillations were recorded during the gas explosions. Based on the pressure recordings from the explosions, the structural damage potential of the pressure was analyzed using shock response spectra. These revealed frequency-dependent dynamic amplifications of relatively high magnitudes. This information must be taken into consideration when designing components and systems that are intended to remain structurally intact and operational in the aftermath of gas explosion events in confined spaces with high aspect ratios, such as tunnels, channels and enclosed passageways.

1. Introduction

Hydrogen is now being introduced as a zero-emission energy carrier in the road, rail and maritime transport sectors, where its successful application will require high safety standards. Intended or accidental releases of hydrogen may cause fires and explosions. Such events are a cause for concern and must be taken into consideration when new technology is introduced. To understand the consequences of gas explosions, a large number of explosion tests with hydrogen and other fuels have been carried out in recent decades, e.g. [1,2], and numerical codes for dispersion, fire, explosion and structural response have been developed and used for scientific and risk analysis, e.g. [3–6].

In simulations of structural response to gas explosions, the standard means of describing load is by idealizing the pressure–time curve to either a triangular shape or an exponentially decaying function with or without negative pressure, e.g. [7–14]. A common misconception is that such events will at most yield a dynamic amplification factor of 2 with respect to static displacements. Based on the Fourier transform and vibration theory, a rectangular pulse is a signal containing frequency components at all frequencies, and a single rectangular pulse will yield a dynamic amplification factor of 2 [15,16]. This holds true as long as the pulse does not contain oscillations. An oscillating pulse may after only a few oscillations far exceed a dynamic amplification factor of 2. The dynamic amplification factor will also be greater than 2 in situations where the structural system contains multiple eigenfrequencies. Under correct conditions, the dynamic amplification from each of these eigenfrequencies will add together and form a total dynamic amplification factor far greater than 2.

For explosions in channels, tunnels or confined spaces with high aspect ratios, and even in vented geometries, explosion pressure may exhibit strong oscillations over several periods for relatively long durations [17,18]. Many structural components installed in such geometries do contain multiple eigenfrequencies.

The aim of this paper is to study the frequency-dependent or dynamic structural damage potential of explosions in inhomogeneous hydrogen-air clouds in tunnel-like geometries. Since various equipment or piping installed in such constructions will have different eigenfrequencies, this study focuses on general behavior. The focus of this work will be on the magnitude of the dynamic amplification factor, with emphasis on highlighting that in several instances this value will be far greater than 2. Our objective is to provide knowledge of this issue for engineers designing and analyzing components and structures that are planned to be installed in tunnel-like geometries. When engineering such components or structures, a common procedure is to perform linear static analyses based on maximum peak load from the explosion to obtain stresses and strains, often using finite element (FE) tools, in order to uncover risk for structural failure of the component or structure. Emulating a dynamic load case, stresses are multiplied by a factor of 2,

* Corresponding author.
E-mail address: magne.bratland@usn.no (M. Bratland).

https://doi.org/10.1016/j.engstruct.2020.111844
Received 15 May 2020; Received in revised form 10 December 2020; Accepted 29 December 2020
Available online 11 January 2021

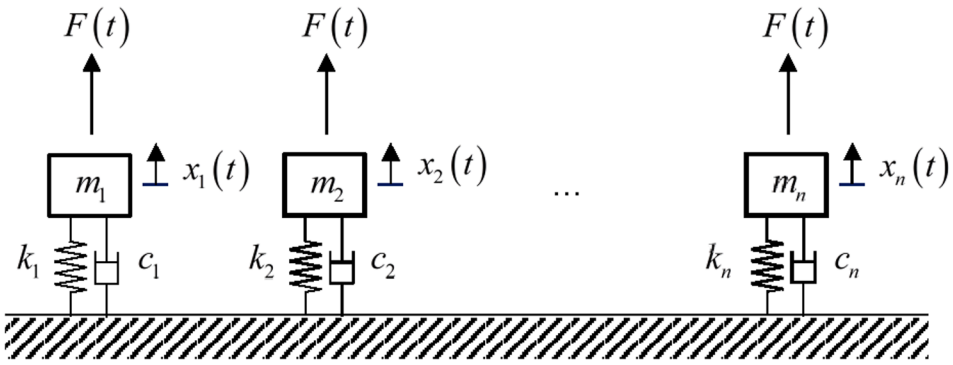

Fig. 1. Set of SDOF mechanical systems subjected to an applied load.

representing the anticipated maximum potential dynamic amplification factor. Knowledge obtained through this work will inform the design and analysis engineer that in some situations, this will be an underestimate of the structural damage potential of the explosion. However, it may not be necessary to perform what are often time-consuming dynamic analyses provided that data on the frequency-dependent structural damage potential of the load and the eigenfrequencies and mode shapes of the relevant components or structures are available. Hence, a linear static analysis combined with for instance modal analysis, both tools commonly available in standard FE software, would be sufficient.

This paper first describes a common method of shock event analysis, and shows how the method can be used to obtain the load characteristics and structural damage potential of an explosion. This is followed by a description of the experimental set-up for the gas explosion tests. Finally, the results in the form of high-speed video images, pressure records, spectrograms, shock response spectra (SRS) and dynamic amplification factors are described and discussed.

2. Shock response spectrum and dynamic amplification factor

In the field of mechanical vibration, *shock* is a term usually used to describe a transient excitation of relatively short duration. The source of the shock may be for instance impact (e.g. drop or crash) or explosions.

One method for characterizing the damage potential of a shock on a mechanical system is to use a so-called shock response spectrum (SRS) [4,16,19–23], which is essentially a graphical representation of the maximum absolute response of a multitude of single-degree-of-freedom (SDOF) systems to a given shock time history. Each SDOF system exhibits a distinct and unique natural frequency, thus enabling a design curve relating inherent system response characteristics to a given shock to be obtained. With this information at hand, the design engineer can relatively easily observe the relevant design-wise high-risk frequency ranges and the consequences of designing a system having natural frequencies within these ranges.

The SRS is often used to analyze the output acceleration, relative velocity or relative displacement in response to an input base excitation acceleration measured using accelerometers [19,23]. However, for a structural system exposed to a sudden and violent change in air pressure caused by above-ground explosions, it is more useful to express the SRS as the absolute displacement to a force input, since data will be recorded using pressure transducers. Pressure is defined as force per area, so converting from pressure to force is a trivial exercise using area as a scaling factor, which in turn will vanish when calculating the dynamic amplification factor.

A force–displacement SRS set-up is illustrated in Fig. 1.

For a mechanical or structural SDOF system exposed to an applied external force, the equation of motion can be written as

$$m\ddot{x}(t) + c\dot{x}(t) + kx(t) = F(t) \tag{1}$$

where m is the mass, c is the damping and k is the stiffness. $x(t)$ is the displacement of the mass m with respect to time. $\dot{x}(t)$ and $\ddot{x}(t)$ are the 1st and 2nd time derivatives of $x(t)$, respectively, i.e. velocity and acceleration of the mass m. $F(t)$ is the applied external force.

If $F(t)$ in Equation (1) is an arbitrary force, the response $x(t)$ in Equation (1) can be found by solving the convolution integral of the product of the force $F(t)$ and the system's impulse response function $h(t)$ as

$$x(t) = F(t) * h(t) = \int_0^t F(\tau)h(t-\tau)d\tau \tag{2}$$

For an SDOF mass-spring-damper system, the system's impulse response function $h(t)$ can be expressed as

$$h(t) = \frac{1}{m\omega_d}e^{-\zeta\omega_n t}sin(\omega_d t) \tag{3}$$

Hence, the response $x(t)$ can be written as

$$x(t) = \frac{1}{m\omega_d}\int_0^t F(\tau)e^{-\zeta\omega_n(t-\tau)}sin[\omega_d(t-\tau)]d\tau \tag{4}$$

where ω_n is the system's natural frequency or undamped eigenfrequency, ω_d is the system's damped eigenfrequency and ζ is the damping ratio.

The static displacement of a linear mechanical SDOF system subjected to a constant load F is given by

$$x_{st} = \frac{F}{k} \tag{5}$$

For an arbitrary and time-varying load $F(t)$, an equivalent static displacement can be written as

$$x_{st} = \frac{F_{max}}{k} = \frac{F_{max}}{m\omega_n^2} \tag{6}$$

since $\omega_n = \sqrt{k/m}$ and hence $k = m\omega_n^2$.

The ratio of dynamic displacement to static displacement is often referred to as *dynamic amplification factor* (sometimes referred to as dynamic load factor or DLF), and is given by

$$R_d = \frac{x(t)}{x_{st}} \tag{7}$$

Inserting Eqs. (4) and (6) into Equation (7) gives

$$R_d = \frac{\frac{1}{m\omega_d}\int_0^t F(\tau)e^{-\zeta\omega_n(t-\tau)}sin[\omega_d(t-\tau)]d\tau}{\frac{F_{max}}{m\omega_n^2}}$$

$$= \frac{\omega_n^2}{F_{max}\omega_d}\int_0^t F(\tau)e^{-\zeta\omega_n(t-\tau)}sin[\omega_d(t-\tau)]d\tau \tag{8}$$

When calculating an SRS, it is customary to express the damping ratio ζ in terms of the maximum steady-state displacement amplitude, or resonant gain, Q for the mass-spring-damper system due to a harmonic force. The peak deformation response is given by

Fig. 2. The experimental rig.

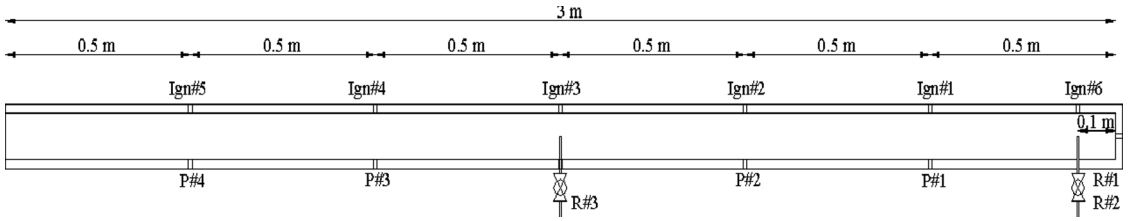

Fig. 3. Schematic diagram showing the ignition locations (Ign#1-Ign#5), pressure transducers (P#1-P#4) and hydrogen inlet locations (R#1-R#3).

$$x_{max} = x_{st} \cdot \frac{1}{2\zeta\sqrt{1-\zeta^2}} \tag{9}$$

which will give the resonant gain Q as

$$Q = \frac{x_{max}}{x_{st}} = \frac{1}{2\zeta\sqrt{1-\zeta^2}} \approx \frac{1}{2\zeta} \text{ for } \zeta \ll 1 \tag{10}$$

When the forcing frequency ω is equal to ω_n, then $x_{max}/x_{st} = 1/(2\zeta)$. The relation between Q and ζ is therefore commonly given [23] as

$$Q = \frac{1}{2\zeta} \text{ or } \zeta = \frac{1}{2Q} \tag{11}$$

Typical values used are $Q = 5$ ($\zeta = 10\%$), $Q = 10$ ($\zeta = 5\%$) and $Q = 50$ ($\zeta = 1\%$). For laboratory simulations, the standard MIL-STD-810G recommends using values for Q of 10 and 50 during processing [24].

An effective algorithm for the calculation of the SRS for a base excitation shock is to use a ramp invariant recursive filter as suggested by Smallwood [25] and as stated in the standard ISO 18431–4 [23]. For a force input shock, the Z-transform of R_d from Equation (8) can be written as

$$H(z) = \frac{b_0 + b_1 \cdot z^{-1} + b_2 \cdot z^{-2}}{1 - a_1 \cdot z^{-1} - a_2 \cdot z^{-2}} \tag{12}$$

with recursion coefficients

$$\begin{aligned} a_1 &= 2e^{-\zeta\omega_n T}\cos(\omega_d T) \\ a_2 &= -e^{-2\zeta\omega_n T} \\ b_0 &= 0 \\ b_1 &= \frac{T\omega_n^2}{F_{max}\omega_d} e^{-\zeta\omega_n T}\sin(\omega_d T) \\ b_2 &= 0 \end{aligned} \tag{13}$$

where T is the sampling time interval. A detailed derivation of the Z-transform with its recursive coefficients can be found in [26].

As stated by Alexander [19], for a system containing multiple degrees of freedom, an estimate of the combined maximum SRS output is typically obtained using a root sum squared type approach taking the mode shapes of the system into consideration.

3. Experimental set-up

The test channel selected was 3 m long, 0.1 m wide and 0.1 m high, open at one end and closed at the other (see Figs. 2 and 3). The channel sidewalls were made of transparent polycarbonate. The experiment was carried out by releasing hydrogen into the channel from a cylinder through 0.25 and 0.5 mm-diameter nozzles. The injection point was either at the closed end-wall or in the middle of the channel. The flow rate was controlled by the backpressure of a regulator valve. Backpressure varied from about 1.2 to 8.0 MPa, corresponding to a hydrogen flow of 15 to 80 L/minute. A continuous ignition source in the form of a high voltage spark was mounted in the upper wall of the channel. Five different ignition locations (Ign#1 to Ign#5) were used as part of the test program, located 0.5, 1, 1.5, 2 and 2.5 m, respectively, from the closed end of the channel. The ignition source was switched on and off in a series of short continuous pulses. Four Kistler 7001 pressure transducers were used to measure explosion pressures, using a sampling rate of 100 kHz. The positions of the four pressure transducers (P#1 to P#4) are shown in Fig. 3. A Photron Ultima APX-RS (black and white) high-speed camera was used to film the experiment, using frame rates of either 1500 or 2000 fps, and a resolution of 1024 × 64 pixels.

4. Experimental results

Since the focus of this paper is to analyze structural response, only a limited number of the experiments are discussed. The aim here is to provide illustrative examples of typical gas explosion scenarios in tunnel-like geometries, and to highlight the anticipated magnitudes of dynamic amplifications. The experiments were not intended as thorough studies of the mechanisms behind the pressure oscillations, and nor were they exhaustive experiments covering all possible variations of parameters such as ignition position, hydrogen flow rate and hydrogen concentration. Emphasis has been placed on demonstrating that dynamic amplifications may well exceed the commonly used value of 2. For this

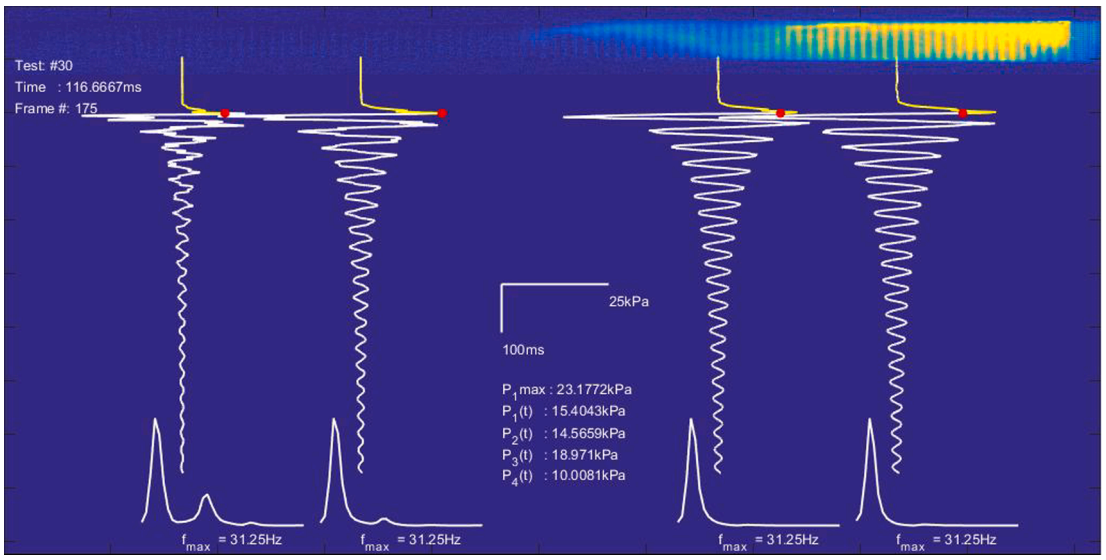

Fig. 4. Frame from the high-speed video of Test #30 (top) with pressure records (center) and power spectra (bottom).

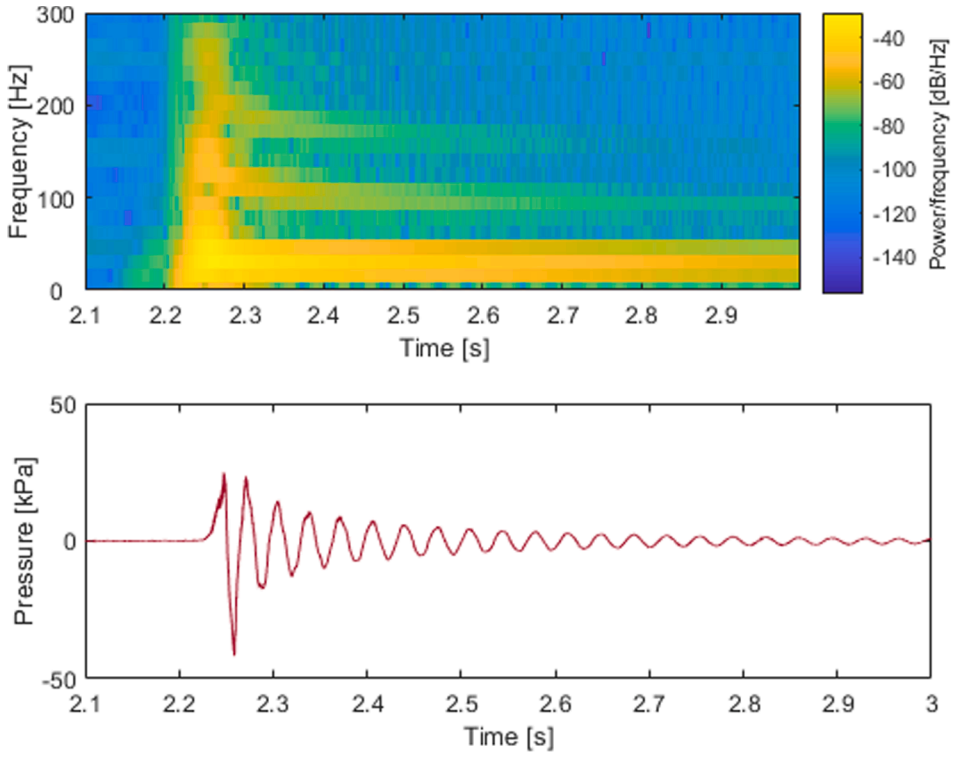

Fig. 5. Spectrogram (top) and time series (bottom) of the pressure record for transducer P#1 from Test #30.

reason, the experiments are deliberately described in quite general terms, with no discussion of factors such as dispersion, flame acceleration and suchlike. It should be noted that the program included several parallel experiments for control and sanity check purposes, all of which revealed similar results and trends in the acquired data. It is also important to bear in mind that the results from these experiments, especially the numerical values of the pressure peaks, are not directly scalable to full-scale scenarios in the real world. However, the underlying physics, i.e. the general behavior of the pressure waves, and specifically the existence of pressure oscillations, is believed to be highly relevant and applicable.

Of a total of 184 experiments carried out, we have selected three typical examples for description. The first, Test #30, had a short ignition distance, and the gas cloud in the upper part of the channel was near-stoichiometric. In Test #150, the cloud was slightly rich and the distance from the jet release to the ignition point was 2 m. In the third test, Test #67, the cloud was very rich and the ignition point was located 2.5 m from the closed end of the tube.

The results are presented in three forms, illustrated by Figs. 4, 5 and 6, respectively. The first, Fig. 4, is an image prepared from the high-speed video and the pressure records. In the upper part of the figure, an image taken from the high-speed video shows the flame front. The middle part of the figure shows four pressure records (from left to right: P#4, P#3, P#2 and P#1, see also Fig. 3) presented as pressure–time

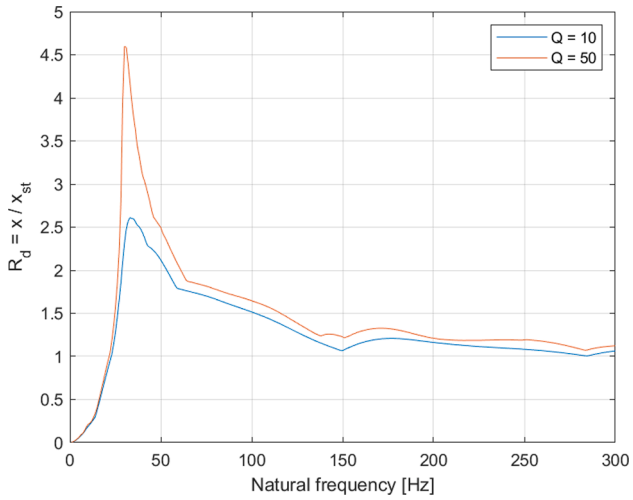

Fig. 6. Absolute displacement SRS with $Q = 10$ and $Q = 50$ for transducer P#1 from Test #30.

diagrams. The time axis is vertical and the scale is given in the middle of the figure. The timescales are 30 ms for Test #67 and 100 ms for Tests #30 and #150. The pressure scale along the horizontal axis is 25 kPa for Test #30 and 10 kPa for Tests #67 and #150. The pressure records are so located in the figure such that they correspond to their positions in the channel in relation to the high-speed video. In this way, the zero pressure values on the axes of the records coincide with the positions of the pressure transducers. Whole pressure records are plotted as white lines. For each pressure record, the red point on the curve marks the pressure and time corresponding to the video image. At the base of the figure, below the pressure curve, a power spectrum is plotted, identifying the frequency of the highest peak.

The second type of figure is shown in Fig. 5. Here, the upper plot is a spectrogram showing frequency and power per frequency vs. time for pressure transducer P#1. The plot is generated using the standard MATLAB function `spectrogram()`, which returns the short-time Fourier transform of the pressure record. The lower plot shows the time series of the pressure record.

The third type of figure is illustrated in Fig. 6 and demonstrates the main result of the analysis. It shows the calculated SRS with $Q = 10$ and $Q = 50$ of the pressure record for pressure transducer P#1. The abscissa of the SRS is the natural frequency (in Hz) of the various SDOF mass-spring-damper systems, while the ordinate represents the dimensionless dynamic amplification factor R_d. Since R_d is the ratio of the calculated response $x(t)$ to the static deformation x_{st}, a value of R_d greater than unity means an amplification of the dynamic response compared to the static response – a phenomenon closely related to resonance. A value of R_d less than unity means a reduction in dynamic response compared to the static response. In such cases, the SDOF mass-spring-damper system has a relatively soft spring and heavy mass, and thus a low natural frequency compared to that of the excitation pulse, and hence responds slowly and moderately to the applied force. This typically occurs in the lower frequency range of the SRS. In the higher frequency range, R_d is typically 1 or close to 1. In such cases, the SDOF mass-spring-damper system has a stiff spring and a light mass and thus a high natural frequency compared to that of the excitation pulse, meaning the pulse frequency is slow and makes the response more or less time-independent, i.e. quasi-static.

4.1. Test #30: Short ignition distance (Ign#1) and near-stoichiometric gas

In Test #30, the distance between the spark and jet nozzle was 0.4 m. The high-speed video showed that the flame propagated directly from the spark and into the turbulent jet without creating pressure oscillations within the channel. The first pressure peak was at 23 kPa, followed by a second at the same level. At the time of the second peak, most of the fuel was combusted and the pressure records showed damped oscillations. It took approximately 13 cycles before the peak was reduced to approximately 10% of the maximum pressure, as shown in Fig. 4.

The results of the spectral analysis are shown in Fig. 5, demonstrating that a single frequency, 30 Hz, dominates the spectrum. This frequency corresponds to the fundamental frequency (first harmonic) of the channel for the speed of sound in air at the initial temperature. This should be expected because only a small part of the channel was filled with the hydrogen-air mixture at the time of ignition during Test #30. Some higher frequencies of approximately 175 and 300 Hz are also seen.

Fig. 6 shows that the SRS shows a maximum dynamic amplification for $Q = 10$ of 2.5 at about 30 Hz. Minor amplifications can also be seen at about 175 Hz and 300 Hz. For $Q = 50$, the largest amplification recorded is about 4.5.

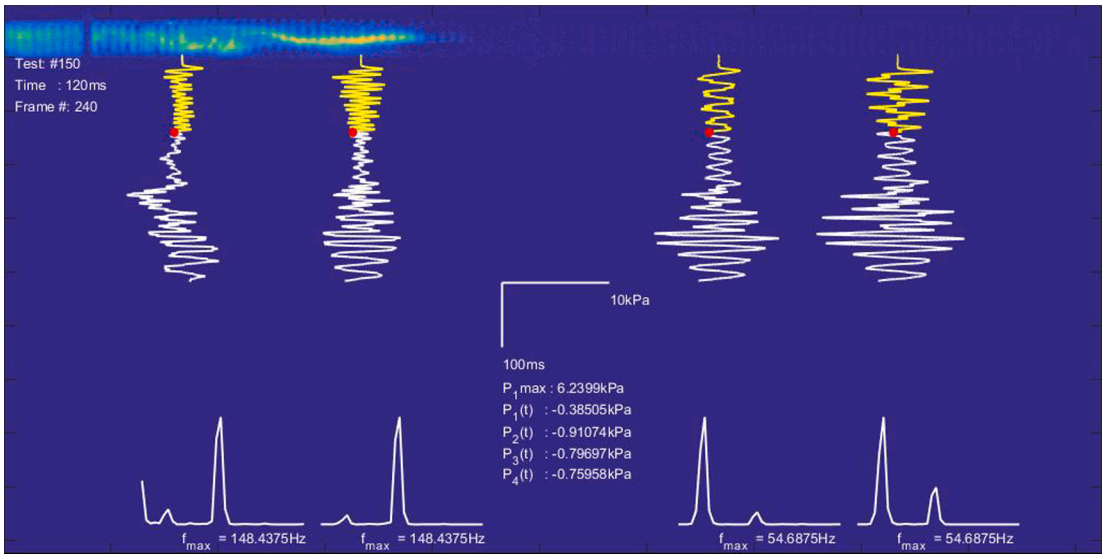

Fig. 7. Frame at 120 ms from the high-speed video of Test #150 (top) with pressure records (center) and power spectra (bottom).

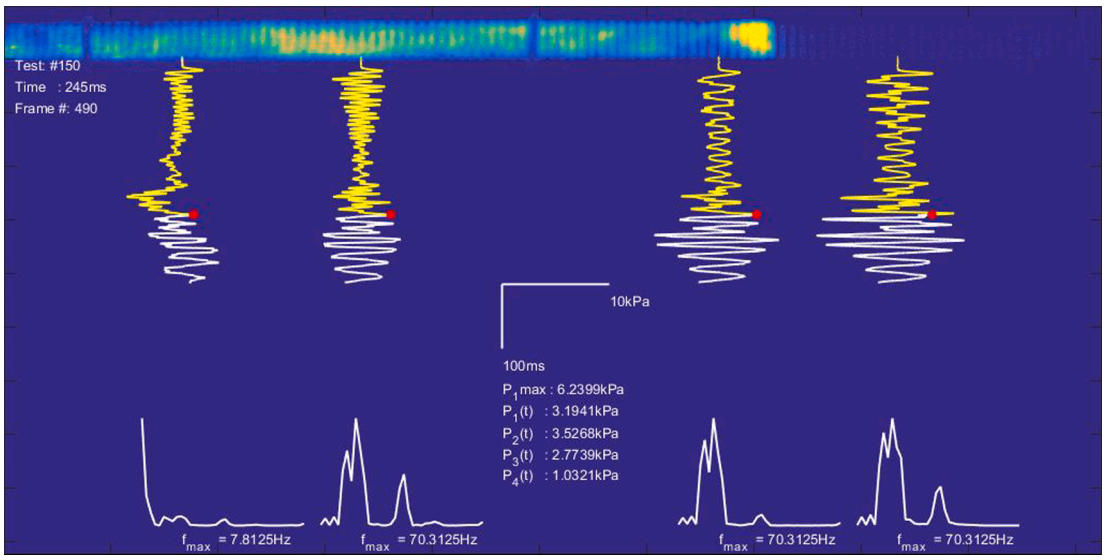

Fig. 8. Frame at 245 ms from the high-speed video of Test #150 (top) with pressure records (center) and power spectra (bottom).

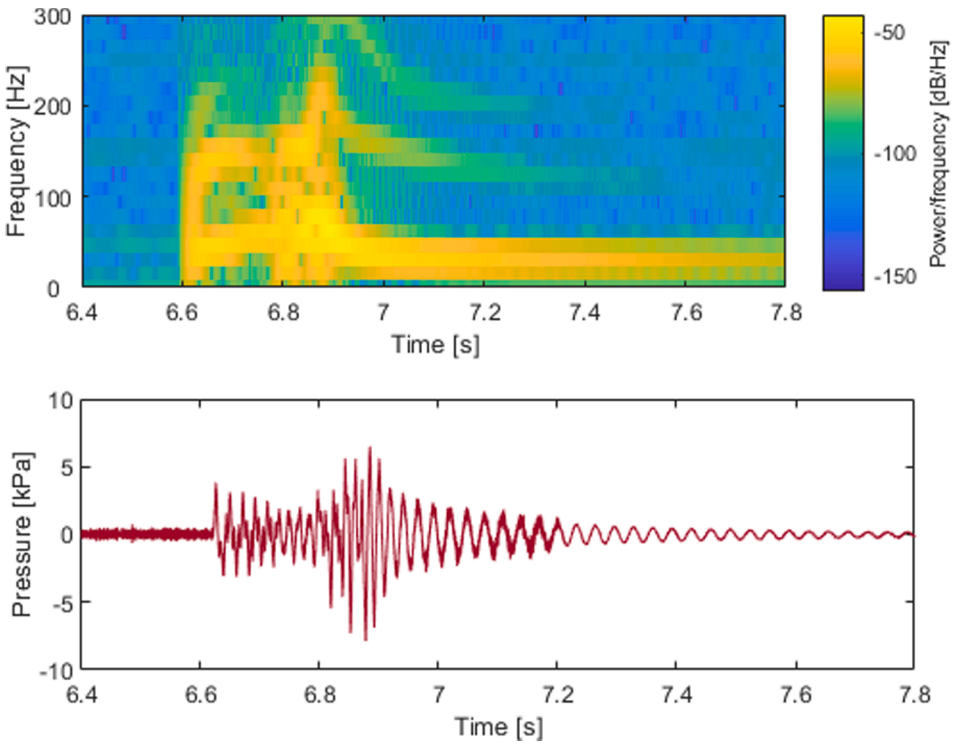

Fig. 9. Spectrogram (top) and time series (bottom) of pressure record for transducer P#1 from Test #150.

4.2. Test #150: Medium ignition distance (Ign#4) and slightly rich gas

In Test #150, the ignition source was placed 2 m from the closed wall and the hydrogen-air gas mixture was slightly rich. The maximum explosion pressure was only 6.2 kPa and the pressure record exhibited a distinctly different behavior from that in Test #30. In this test, the oscillations start at an early phase of flame propagation, and several periods of pressure oscillations can be seen as the flame propagates into the channel. Fig. 7 shows that the pressure oscillation frequency at transducers P#1 and P#2, positioned in reactants (i.e. fuel–air), peaks at 54 Hz. For transducers P#3 and P#4 (in products), the peak is recorded at 148 Hz.

During the first 200 ms of flame propagation after the first pressure peak, the pressure oscillations are slightly damped. This is seen most clearly at pressure transducer P#3. When the flame reaches 1 m from the closed end, the oscillations are strongly amplified. This is a well-known phenomenon in homogeneous pre-mixed fuel–air mixtures when the flame propagates in tubes with open and closed ends following ignition at the open end. A classic experiment of this type is described in reference [17], where strong oscillations in pressure are observed when the flame has propagated to about two-thirds of the length of the tube. In Fig. 8, the flame has reached about two-thirds of the length of the 3-meter channel. The amplification of the pressure oscillations can be clearly seen, and the peak pressure oscillation frequencies have shifted to 70 Hz.

The spectrogram in Fig. 9 shows that during the first 200 ms after

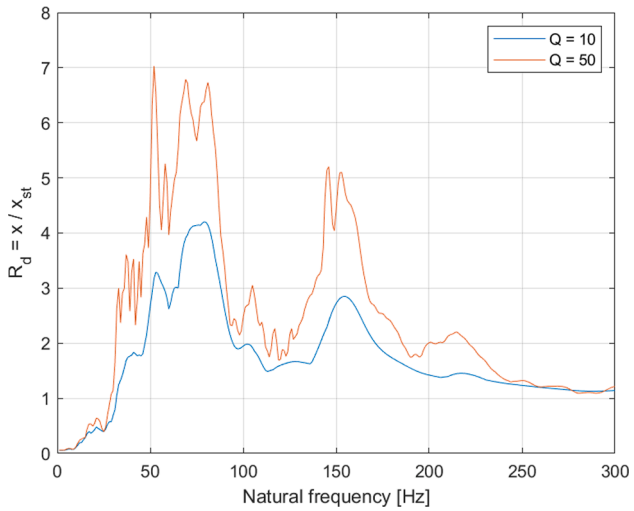

Fig. 10. Absolute displacement SRS with $Q = 10$ and $Q = 50$ for transducer P#1 from Test #150.

ignition, the peak frequency increases more or less linearly with time from 50 to 70 Hz. This can be explained by the increase in the speed of sound as the flame burns through the channel and fills it with hot combustion products. It is also interesting to note that after 7 s, once the fuel is consumed, the first harmonic frequency settles rapidly to 40 Hz.

The SRS plot in Fig. 10 for $Q = 50$ shows three main peaks. The first is a narrow peak at 50 Hz, followed by two local peaks at between 70 and 80 Hz, and two at around 150 Hz. The R_d values for these peaks are about 7, 6.8 and 5.2, respectively. The SRS for $Q = 10$ exhibits peaks at the same frequencies as for $Q = 50$. However, the peak R_d value at 50 Hz is reduced by significantly more than those at between 70 and 80 Hz and 150 Hz. This is probably due to the narrow width of the 50 Hz peak, making its value more sensitive to damping.

4.3. Test #67: Long ignition distance (Ign#5) and very rich gas

In Test #67, the gas cloud was very rich with an estimated average concentration of 60 to 70% H_2. The ignition point was 2.5 m from the closed wall. As is illustrated in Fig. 11, the peak pressure achieved was 41 kPa. The high-speed video shows rapid flame propagation through the channel, with the flame filling the entire cross-section and not only the upper part. During this test, a localized explosion occurred when the flame reached about two-thirds along the length of the channel.

Fig. 12 shows the pressure spectrogram and time series for transducer P#1. The pressure record shows a relatively high peak at 41 kPa, but only three cycles are required to damp the peak and reduce the amplitude by a factor of 10. This rapid decay in pressure results in relatively low values for the SRS plots shown in Fig. 13. The maximum values are about 3.6 for $Q = 50$ and 2.5 for $Q = 10$.

5. Discussion

The power spectra and SRS plots presented in the previous section coincide well, identifying similar maximum pressure frequencies and frequency bandwidths (narrow or broad), as should be expected. However, the information obtained from the SRS, which is not easily available from the power spectrum, is the expected maximum dynamic amplification. The SRS does not give a definite answer to what the dynamic amplification will actually be, mainly due to the inherent difficulty of estimating the damping in mechanical or structural systems. This can be seen in the difference between the SRS plots for $Q = 10$ and $Q = 50$. However, it does provide a good indication of the magnitudes of dynamic amplification that can be expected.

As noted in the introduction, there is a common misconception that dynamic amplification will never be greater than 2 for an SDOF system. This probably stems from the fact that in an undamped SDOF system, a rectangular pulse will yield a maximum dynamic amplification of 2, and any other non-oscillatory pulse (half-sine, triangular, exponential, etc.) will yield amplifications below this value, c.f. [16]. However, this does not hold true for oscillatory pulses. As is demonstrated by Equation (10), the limiting value of dynamic amplification is in fact Q. For an undamped system, Q is infinite because ζ is zero. It is worth mentioning here that of all the 184 experiments, only very few exhibited a dynamic amplification factor of 2 or less for $Q = 10$. Typical values were between 2.5 and 4, with the highest value close to 10.

A discussion about dynamic amplification and positive peak pressure may be appropriate here. A comparison of the three SRS curves from Tests #30, #67 and #150, where $Q = 10$, is shown in Fig. 14.

As can be seen in Fig. 14, Tests #30 and #67 yielded similar maximum dynamic amplification values, albeit at different frequencies (about 30 and 70 Hz, respectively), while Test #150 yielded almost twice the dynamic amplification of Tests #30 and # 67. This may appear as strange since both Test #30 and #67 recorded much higher positive peak pressures (23 and 41 kPa, respectively) compared to Test #150

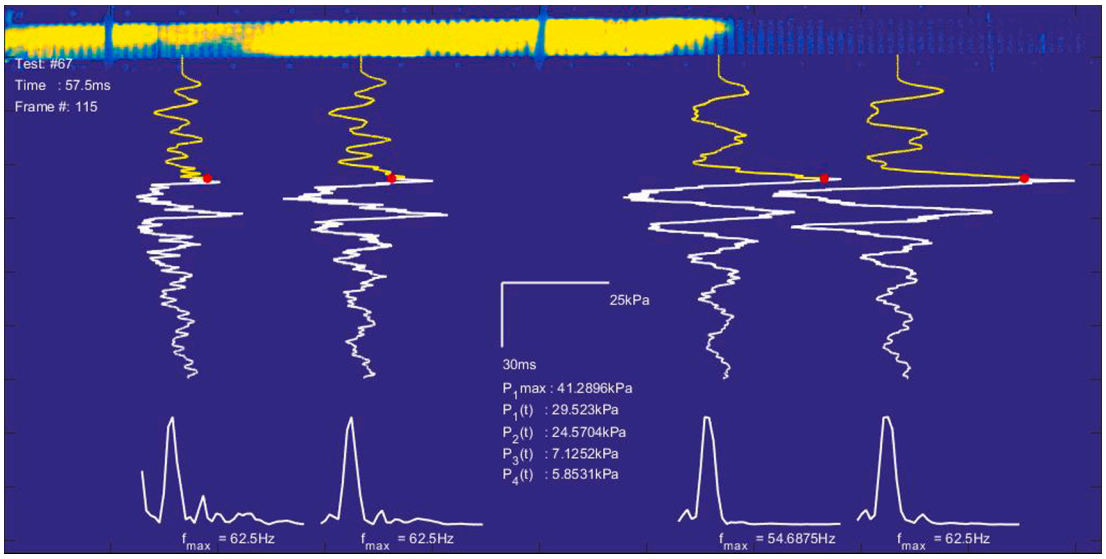

Fig. 11. Frame from the high-speed video of Test #67 (top) with pressure records (center) and power spectra (bottom).

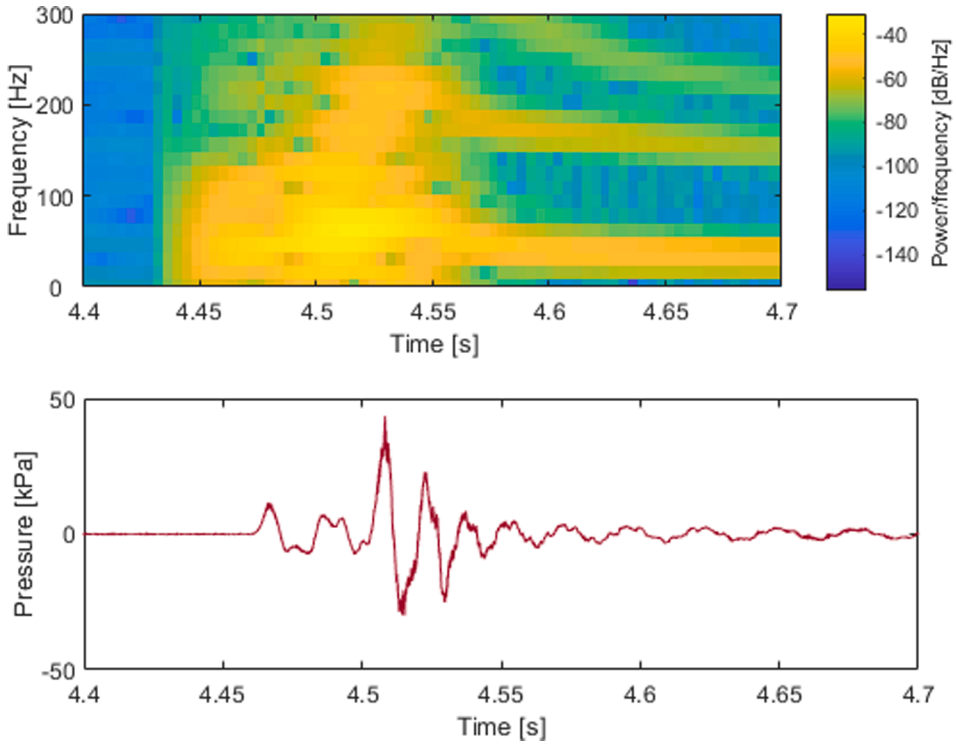

Fig. 12. Spectrogram (top) and time series (bottom) of pressure record for transducer P#1 from Test #67.

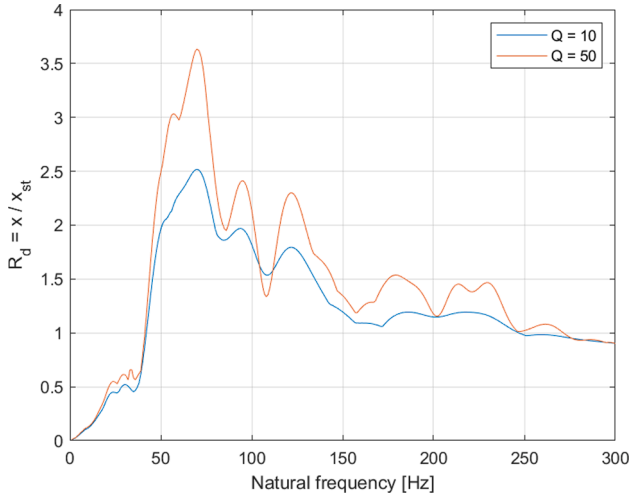

Fig. 13. Absolute displacement SRS with $Q = 10$ and $Q = 50$ for transducer P#1 from Test #67.

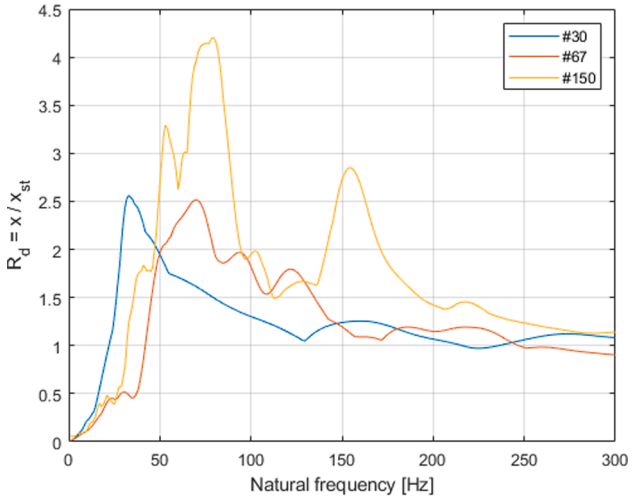

Fig. 14. Absolute displacement SRS with Q = 10 for transducer P#1 from Tests #30, #67 and #150.

(6.2 kPa). For comparison, the three time-pressure curves are shown in Fig. 15.

Returning to Equation (7), which shows that the dynamic amplification factor is the ratio of dynamic to static displacement, it makes sense to normalize the time-pressure curves shown in Fig. 15. Such a normalization is shown in Fig. 16.

Fig. 16 shows that Test #150 exhibits far more normalized high-value pressure oscillations compared to Tests #30 and #67. In addition, the decay rate of the oscillations in Test #150 is less than that for Tests #30 and #67. All this contributes to making the dynamic amplification recorded in Test #150 much greater than that for Tests #30 and #67. However, this does not mean that Test #150 will generate the greatest overall displacements (and thus the greatest strains and stresses) for a structural system. These will be governed by both the static displacement and the dynamic amplification factor.

As can be seen in Figs. 15 and 16, Tests #30 and #67 both exhibit strong pressure peaks, although the oscillations recorded in Test #30 are not dampened as quickly as in Test #67. In Test #67, the gas in the channel is described as light, comprising hot combustion products and/or a high fraction of hydrogen. In Test #30, however, the gas is mostly cold air with a higher density. More mass is thus in oscillation in Test #30 than in Test #67. Differences in viscosity may also influence the damping.

6. Conclusions

In this paper, we have presented a structural response analysis from gas explosion tests in a 3-meter channel containing inhomogeneous

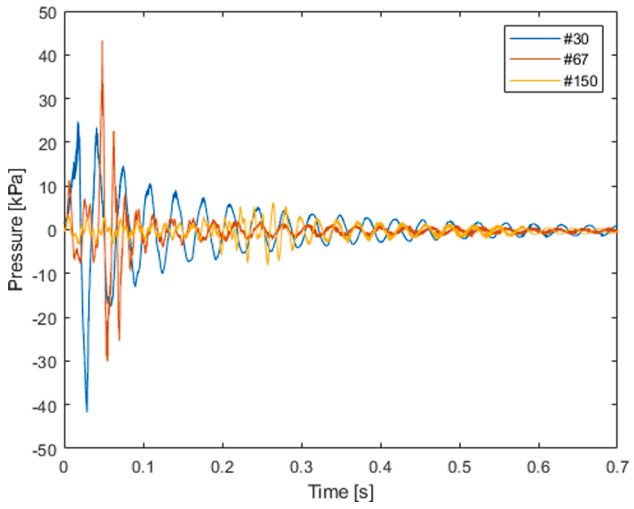

Fig. 15. Time-pressure curves for transducer P#1 from Tests #30, #67 and #150.

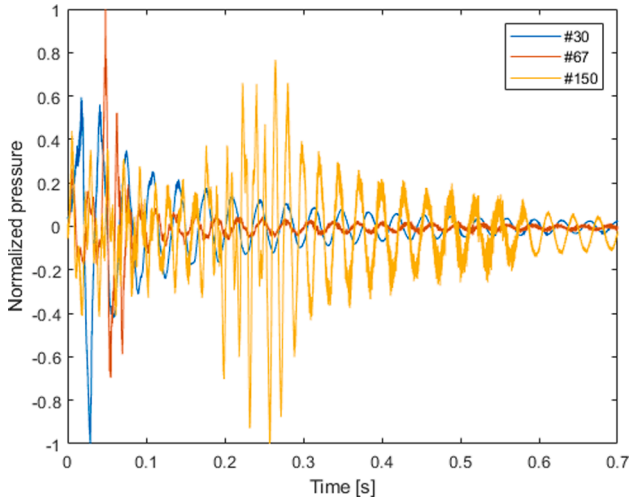

Fig. 16. Normalized time-pressure curves for transducer P#1 from Tests #30, #67 and #150.

hydrogen-air mixtures. Time series plots and spectrograms of the pressure records show strong pressure oscillations over several cycles. A structural response analysis based on shock response spectra shows that we may anticipate dynamic amplifications well above the commonly used value of 2.

It is important to be aware of these phenomena when designing equipment, such as ventilation fans, for use in tunnels, channels or compartments with high aspect ratios, and in particular equipment that is intended to function in the aftermath of a gas explosion incident. Strong and relatively prolonged pressure oscillations may cause structural damage to, and ultimately the failure of, critical components.

CRediT authorship contribution statement

Magne Bratland: Conceptualization, Methodology, Formal analysis, Writing - original draft, Writing - review & editing. **Dag Bjerketvedt:** Conceptualization, Methodology, Formal analysis, Writing - original draft, Writing - review & editing, Funding acquisition. **Knut Vaagsaether:** Conceptualization, Methodology, Formal analysis, Writing - original draft, Writing - review & editing, Funding acquisition.

Declaration of Competing Interest

The authors declare that they have no known competing financial interests or personal relationships that could have appeared to influence the work reported in this paper.

Acknowledgements

This study was carried out as part of MoZEES, a Norwegian Centre for Environment-friendly Energy Research (FME), co-sponsored by the Research Council of Norway (project number 257653) and 40 partners from the research, industrial and public sectors. The authors take the opportunity to acknowledge the contribution to this work by Kanshan Rai during conduct of the experiments.

References

[1] Bjerketvedt D, Bakke JR, Van Wingerden K. Gas explosion handbook. J Hazard Mater 1997;52:1–150.
[2] Cirrone D, Shentsov V, Kashkarov S, Dadashzadeh M, Makarov D, Molkov V, Markert F, Giuliani L, Venetsanos A, Giannissi S, Tolias I, Kuznetsov M, Jordan T, Xu Z, Russo P, Vaagsaether K, Van Esbroeck T, De Backer N, Braune C, van den Berg J, de Jong F, Grune J, Bernad A. Deliverable 1.2 Report on hydrogen hazards and risks in tunnels and similar confined spaces. HyTunnel-CS: Fuel Cells and Hydrogen Joint Undertaking; 2019.
[3] Baker WE, Cox PA, Kulesz JJ, Strehlow RA, Westine PS. Explosion Hazards and Evaluation. Saint Louis: Elsevier Science & Technology; 1983.
[4] Krauthammer T. Modern protective structures. Boca Raton, Fla: CRC Press; 2008.
[5] ABS Consulting Ltd. Design, materials and connections for blast-loaded structures. Research Report 405: UK Health and Safety Executive. 2006.
[6] Li Y, Xiao J, Zhang H, Breitung W, Travis J, Kuznetsov M, et al. Numerical analysis of hydrogen release, dispersion and combustion in a tunnel with fuel cell vehicles using all-speed CFD code GASFLOW-MPI. Int J Hydrogen Energy 2020.
[7] Krauthammer T, Altenberg A. Negative phase blast effects on glass panels. Int J Impact Eng 2000;24:1–17.
[8] International Organization for Standardization. ISO 16933:2007 - Glass in building — Explosion-resistant security glazing — Test and classification for arena air-blast loading. 2007.
[9] Ngo T, Mendis P, Gupta A, Ramsay J. Blast loading and blast effects on structures–an overview. Electronic Journal of Structural Engineering. 2007;7:76–91.
[10] Li J, Hao H. Development of a simplified numerical method for structural response analysis to blast load. Procedia Eng 2011;14:2558–66.
[11] Bedon C, Amadio C, Sinico A. Numerical and analytical investigation on the dynamic buckling behavior of glass columns under blast. Eng Struct 2014;79:322–40.
[12] Rigby S, Tyas A, Bennett T. Elastic–plastic response of plates subjected to cleared blast loads. Int J Impact Eng 2014;66:37–47.
[13] Kang K-Y, Choi K-H, Choi JW, Ryu YH, Lee J-M. An Influence of Gas Explosions on Dynamic Responses of a Single Degree of Freedom Model. Shock Vib 2016.
[14] Shepherd JE. Structural response of piping to internal gas detonation. J Pressure Vessel Technol 2009;131.
[15] Kreyszig E. Advanced Engineering Mathematics. 8th ed: Inc: John Wiley & Sons; 1999.
[16] Thomson WT, Dahleh MD. Theory of Vibration with Applications. 5th ed. Upper Saddle River, N.J., USA: Prentice Hall, Inc.; 1998.
[17] Guénoche H. Chapter E - Flame Propagation in Tubes and in Closed Vessels. In: Markstein GH, editor. AGARDograph, vol 75: Nonsteady Flame Propagation: Elsevier; 1964. p. 107-81.
[18] Heidari A, Wen J. Flame acceleration and transition from deflagration to detonation in hydrogen explosions. Int J Hydrogen Energy 2014;39:6184–200.
[19] Alexander JE. Shock response spectrum-a primer. Sound & vibration. 2009;43:6–15.
[20] Palm WJ. Mechanical Vibration. Hoboken, N.J., USA: John Wiley & Sons, Inc.; 2007.
[21] Chopra AK. Dynamics of structures: Theory and applications to earthquake engineering. 3rd ed. Upper Saddle River, N.J: Pearson Prentice Hall; 2007.
[22] Allan GP, Thomas LP. Harris' Shock and Vibration Handbook. 6th ed. New York: McGraw-Hill Education; 2010.
[23] International Organization for Standardization. ISO 18431-4:2007 - Mechanical vibration and shock — Signal processing — Part 4: Shock-response spectrum analysis. 2007.
[24] United States Department of Defense. MIL-STD-810G. Environmental Engineering Considerations and Laboratory Tests. 2008.
[25] Smallwood DO. An improved recursive formula for calculating shock response spectra. Shock and Vibration Bulletin. 1981;51:211–7.
[26] Irvine T. An introduction to the shock response spectrum. Vibrationdata: Rev S; 2012.